10
FERMILAB
MAR 1 2 1999
LIBRARY
ISAS-RN-672

ISAS RESEARCH NOTE

ISAS RN 672

Improvement of the position resolution of the CCD for X-ray use

K. Yoshita[1], H. Tsunemi[1,2,3], E. Miyata[1,2],
K.C. Gendreau[1], and M.W. Bautz[5]

Fermilab Library
0 1160 0068528 3

NAME	ID No.	M.S.

THE INSTITUTE OF SPACE AND ASTRONAUTICAL SCIENCE

THE INSTITUTE OF SPACE AND ASTRONAUTICAL SCIENCE
YOSHINODAI, SAGAMIHARA, KANAGAWA 229-8510

ISAS RESEARCH NOTE

ISAS RN 672

Improvement of the position resolution of the CCD for X-ray use

K. Yoshita[1], H. Tsunemi[1,2,3], E. Miyata[1,2],
K. C. Gendreau[4], and M. W. Bautz[5]

February 1999

[1] *Department of Earth and Space Science, Graduate School of Science, Osaka University, Machikaneyama, Toyonaka, 560-0043*
[2] *CREST, Japan Science and Technology Corporation (JST)*
[3] *The Institute of Space and Astronautical Science Yoshinodai, Sagamihara, Kanagawa, 229-8510*
[4] *NASA/GSFC* NASA, Goddard
[5] *Massachusetts Institute of Technology* MIT

To appear in IEEE Trans. Nucl. Sci., Vol 46, No. 2, 1999

Improvement of the position resolution of the CCD for X-ray use

K. Yoshita[a,1], H. Tsunemi[a,b], E. Miyata[a,b], K. C. Gendreau[c] and M. W. Bautz[d]
[a] Department of Earth and Space Science, Graduate School of Science, Osaka University, Machikaneyama, Toyonaka, 560-0043, Japan
[b] CREST, Japan Science and Technology Corporation (JST)
[c] NASA/GSFC
[d] Massachusetts Institute of Technology

Abstract—
We report here experimental results relating X-ray interaction location and event splitting. The X-ray interaction location can be localized at subpixel scale using the mesh technique. We found that the center of gravity of the split event is well-correlated with the X-ray interaction location. We analyzed the data using two models for the charge cloud shape: one is the Rectangular model and the other is the Gaussian model. Although we could not distinguish between these models, we measured a root-mean-square charge cloud size of $1 \sim 2\mu$m for X-rays of Y-L (1.9 keV), Ag-L (3.0 keV) and Ti-K (4.5keV). When the X-rays enter near the pixel boundary, the charge splits into adjacent pixels, allowing determination of the X-ray interaction location with an accuracy of $1.5 \sim 2.2\mu$m. We, therefore, expect that the X-ray CCD can function as an X-ray imager with subpixel resolution, which will be especially useful in applications involving very high spatial resolution optics.

Keywords— **charge-coupled-device, mesh experiment, sub-pixel resolution, charge cloud shape**

I. Introduction

THE direct X-ray photon detection charge coupled device (CCD) has become widely used in X-ray astronomy [1]. It has medium energy resolution and good spatial resolution. The spatial resolution is primarily determined by the pixel size. There are several satellite programs employing the CCD as an X-ray photon count detector: ASCA [2], AXAF [3], [4], XMM [5], [6], ASTRO-E [7], JET-X [8], ABRIXAS [9], [10]. Table I summarizes the CCD characteristics used for them. The image size given by the product of the focal length and the half power diameter is also listed.

When an X-ray photon enters the CCD, a number of electrons are produced through the photoabsorption process. When the photoabsorption occurs inside the depletion region, the entire charge cloud is pulled to the potential well generated by the gates. The charge cloud size expands through the diffusion process. Although it is much smaller than the CCD pixel size, the entire charge cloud is not always collected in a single pixel. If the X-ray interaction position is well away from the pixel boundary, the entire charge cloud is collected into one pixel forming a single event. If the X-ray interaction position is close enough to the pixel boundary, a part of the charge cloud spills over the boundary forming a split event. If it is near the pixel corner, it will form a 3–4 pixel split event. Taking into account the charge cloud size in the X-ray energy range of interest (below 10 keV), the X-rays absorbed in the depletion region split into at most 4 pixels. In other words, the split event can be at most 4 pixels in size if the photon interacts in the depletion region.

TABLE I
CCD characteristics for X-ray astronomy

	Pixel size (μm)	Image size (μm)
ASCA SIS	27	3000
AXAF ACIS	24	25
XMM EPIC	40	550
XMM PN-CCD	150	550
ASTRO-E XIS	24	2800
JET-X	27	340
ABRIXAS	150	470

When the photoabsorption occurs in the electric field free region below the depletion region, the charge moving downward will be reflected in an epitaxial structure and will be lost in a device constructed on bulk silicon while the charge moving upward will enter the depletion region collected in the potential well. The collected charge will form a large cloud resulting in a multi-pixel event, more than 4 pixel event in general. Therefore, an event occupying many pixels does not represent the incident X-ray energy.

In any case, one X-ray photon generates 'an island': a series of some number of contiguous pixels having some amount of charge. Practically, we consider the pixel as having signal if its output is larger than the

Manuscript received August 17, 1998; accepted January 4, 1999.
[1] Partially supported by JSPS Research Fellowship for Young Scientists, Japan.

split threshold, T_{split}. So far, the pixel having the maximum charge within the island is called 'the event pixel'. This pixel is considered to be the X-ray interaction position. Therefore, positional accuracy is no better than the size of the pixel.

Recently, a new technique has been introduced to obtain the X-ray response of the CCD with sub-pixel resolution [11]. The new technique employs a parallel X-ray beam and a metal mesh placed just above the CCD. The mesh is a metal film containing small holes with periodic spacing. The hole size, which is smaller than the CCD pixel size, determines the attainable spatial resolution. The mutual relation between the CCD and the mesh hole can be determined by referring to the moire pattern obtained in this experiment. There are two types of experiments: a single-pitch mesh and a multi-pitch mesh [12]. The single-pitch mesh experiment employs a mesh whose hole spacing is equal to that of the CCD pixel size. The multi-pitch mesh experiment employs a mesh whose hole spacing is a multiple of that of the CCD pixel size. The single-pitch mesh experiment clearly showed that the X-rays entering away from the pixel boundary formed single events. The X-rays entering near the pixel boundary formed split events. Using the single-pitch mesh experiment, we can unambiguously determine the interaction position of single events. However, we can not always determine the interaction position of split events.

The single event has only the information that the X-ray entered somewhere in the pixel. The accuracy of the position information is limited by the pixel size. However, the split event has more detailed information on the interaction position. Since we know the shape of the charge cloud from the multi-pitch mesh experiment [12], we can improve the position information of the X-ray interaction position, particularly for the split events. This paper describes the experimental results to improve the X-ray interaction position using the backup CCD [13] camera system of the ASCA satellite.

II. Experimental Setup

We performed the single-pitch mesh experiment described in detail by Yoshita et al. [14]. It consisted of the pseudo-parallel X-ray beam and a metal mesh placed just above the CCD chip. The X-ray beam divergence is 250μrad. The CCD is a backup system for the ASCA SIS [13]. It consists of 422×420 pixels with 27μm square. The mesh is made of copper of $10\,\mu$m thickness and has small holes with periodic spacing of 27μm. We measured the hole size using a SEM and found it to be about 5.6μm in diameter.

We used characteristic X-rays of: Y-L (1.9 keV), Ag-L (3.0 keV) and Ti-K (4.5 keV). The higher energy X-rays can penetrate the copper foil, which made it difficult to localize the interaction position for them. We obtained the X-ray responsivity of the CCD with subpixel resolution [14]. T_{split}, the split threshold, was set to $120eV$ through this paper unless otherwise specified.

We obtained the precise spatial relation between the CCD and the metal mesh and reconstructed the pixel image. Figure 1 shows the distribution of various types of X-ray events inside the pixel. It clearly shows that the single events occur when the X-ray interaction position is well within the pixel boundary while the split events occur when the X-ray interaction position is close to the pixel boundary such that the charge spills over the adjacent pixel. Based on this figure, we can easily understand that the interaction position of the X-ray event can be determined to better than the pixel size. Pivovaroff et al. [15] proposed a similar idea using the mesh experiment for the AXAF CCD (24μm square pixel): that the CCD pixel could be divided into mini-pixels each of which corresponded to the individual pattern of the island.

III. Data Analysis

Since the experiment we performed is a single-pitch mesh experiment, we can not uniquely determine the interaction position for all the X-ray events. The nearest mesh hole location to any position on the CCD is surely less than half the pixel size. When we detect the X-ray event, we specify the event pixel which has the biggest signal out of the pixels in the island. If we assume that the center of the event pixel is the X-ray interaction position, we always see that the nearest hole position is within the half pixel size. In some cases, the second nearest hole is almost the same distance to the center of the event as the first nearest hole. There are many cases in which we can not determine the true hole through which the X-ray entered.

When we employ the multi-pitch mesh, we can determine the X-ray interaction position both for single events and for split events. Tsunemi et al. [16] proposed a method to obtain the charge cloud shape using all the X-ray events based on the multi-pitch mesh experiment. However, we can not use their method, since we used a single-pitch mesh. Therefore, we look for another method to determine the charge cloud shape.

A. *Pixel outputs of the split event*

We estimate the size of the charge cloud shape from the effective width of the region where the two-pixel split events are formed [14]. By using the multi-pitch mesh experiment, Tsunemi et al. [16] determined the charge cloud shape. These results show that the charge cloud shape can be well represented by a Gaussian function with different width along X and Y axes. The charge cloud size is a few μm in size which is smaller than the pixel size we used. It is also confirmed that there are substantial fraction of

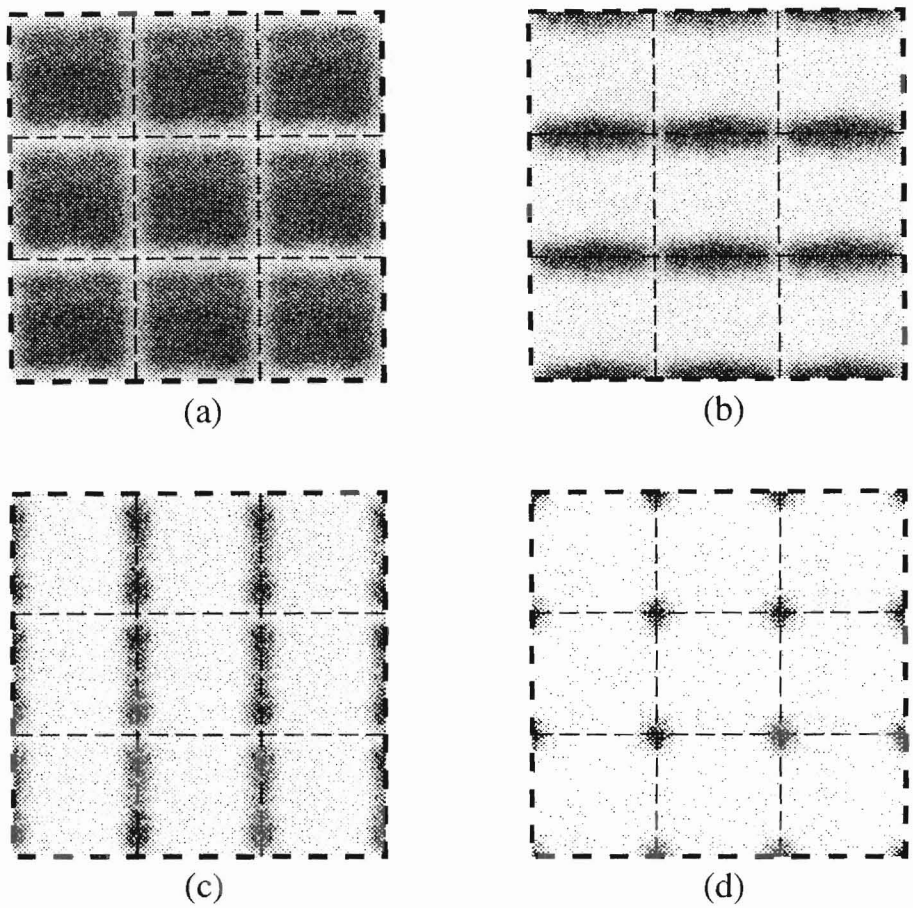

Fig. 1. The mesh experiment reveals the X-ray interaction position with subpixel resolution: (a) for single events, (b) for vertically split events, (c) for horizontally split events and (d) for 3–4 pixel split events. These are the results of Y-L X-rays (1.9 keV). The dashed lines represent the pixel boundary.

the X-ray photons forming single events, which show that the charge cloud size is much smaller than the pixel size. Therefore, we can safely assume that the charge will split into at most four pixels.

We represent the charge cloud shape by the function of $f(X - X_{in}, Y - Y_{in})$ given in eq.(1) where (X_{in}, Y_{in}) is the X-ray interaction position.

$$f(X,Y) = S(\sigma_X, X)S(\sigma_Y, Y) \quad (1)$$

where S denotes the charge cloud shape in one dimension, σ_X and σ_Y are the standard deviation of the shape along X and Y axes when the photoabsorption occurs at the characteristic interaction depth. We assume that $S(\sigma, X)$ is normalized such that $\int S(\sigma, X)dX$ becomes unity.

The output from the nth pixel, $Pixel_n(X_{in}, Y_{in})$, is given in eq.(2)

$$Pixel_n(X_{in}, Y_{in}) = \int_{Y_{n-1}}^{Y_n} \int_{X_{n-1}}^{X_n} f(X - X_{in}, Y - Y_{in}) dX dY \quad (2)$$

where $(Y_{n-1}, Y_n, X_{n-1}, X_n)$ denotes the boundary of the nth pixel. Since the cloud shape is assumed to be a product of the function of X and that of Y, we can independently treat X and Y. Therefore, we will focus on the one dimensional case.

The outputs of the (n+1)th and nth pixel are given below.

$$D_{n+1}(X_{in}) = \int_{X_n}^{X_{n+1}} S(\sigma_X, X - X_{in}) dX \quad (3)$$

$$D_n(X_{in}) = \int_{X_{n-1}}^{X_n} S(\sigma_X, X - X_{in}) dX \quad (4)$$

We should note $D_{n+1} + D_n = 1$. If X_n is the nearest pixel boundary to X_{in}, the entire primary charge will be collected either in the nth or the (n+1)th pixel. If X_{in} is far away from X_n, it will form a single event. If X_{in} is close enough to X_n, the charge will split into two pixels.

B. *Center of gravity of the split event*

Tsunemi et al. [12] showed that the center of gravity of the split event denoted much finer interaction position than the pixel size while that of the single event denoted it with the pixel size. Since they employed the CCD with 12μm pixel size, the center of

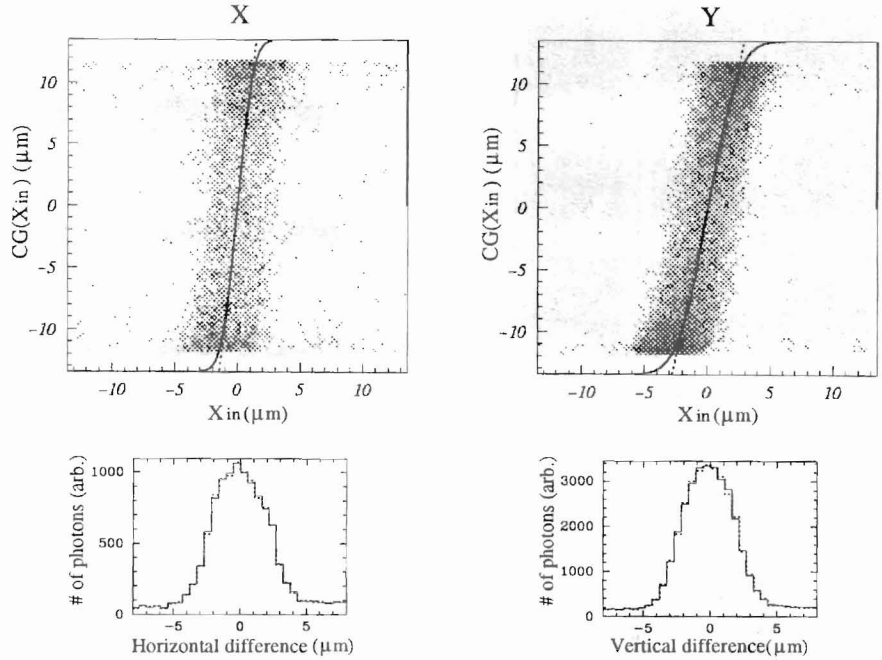

Fig. 2. The upper panel shows the relation of X-ray events for Y-L X-rays between X_{in} and $CG(X_{in})$. The lower panel shows the residual between the data and the best fit models. The solid line represents the best fit Gaussian model while the dotted line represents the best fit Rectangular model.

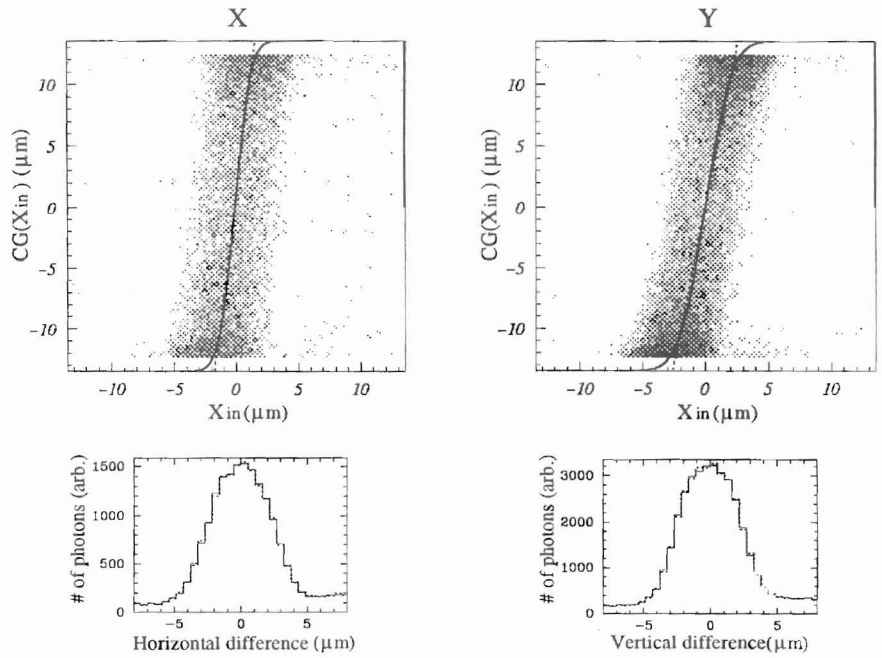

Fig. 3. Same as that for Fig. 2 but for Ag-L X-rays.

gravity shows accurate interaction position. However, the pixel size we used is 27μm, which may not allow so accurate an interpolation.

In principle, the mesh technique can determine the X-ray interaction position with subpixel resolution if we can determine which hole each X-ray really enters. In practice, however, the mesh technique can not, in general, determine which hole the X-ray actually enters. If we regard the event pixel as the X-ray interaction position, the position accuracy will be equal

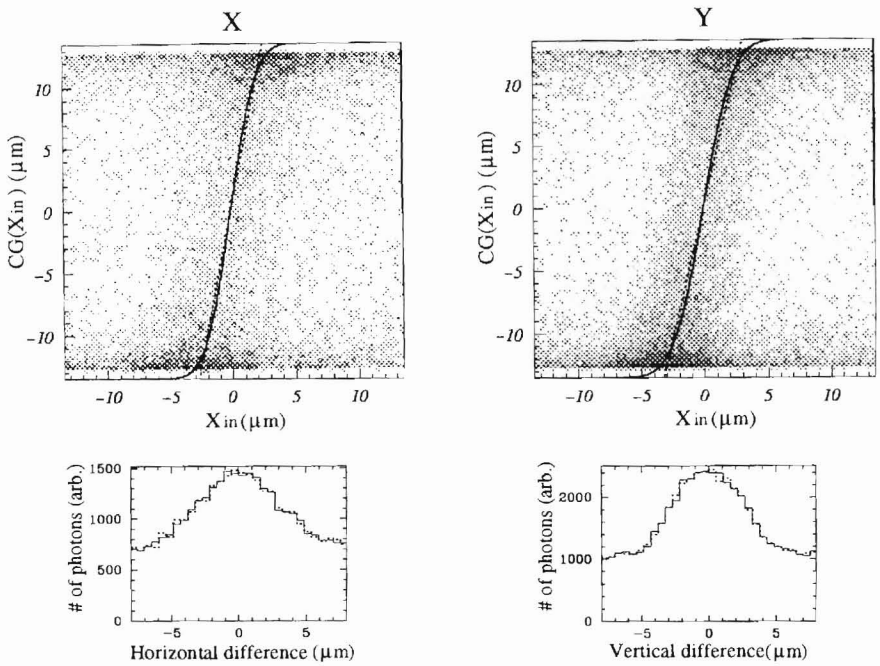

Fig. 4. Same as that for Fig. 2 but for Ti-K X-rays. Due to the penetration power of X-rays, the background level becomes substantially high.

to the pixel size. This accuracy is not enough to unequivocally identify the hole in the single-pitch mesh experiment. However, the center of gravity of split events can determine the interaction position to better than the pixel size. Therefore, we can uniquely determine the interaction position only for split events.

We calculate the center of gravity, $CG(X_{in})$, of the X-ray event weighted by the charge in each pixel given below.

$$\begin{aligned} CG(X_{in}) & \\ &= D_n(X_{in})\frac{X_{n-1}+X_n}{2} + D_{n+1}(X_{in})\frac{X_n+X_{n+1}}{2} \\ &= X_n + \frac{D_{n+1}(X_{in}) - D_n(X_{in})}{2}L \\ &= \frac{L}{2} - L\int_{-\infty}^{-X_{in}} S(\sigma, X)dX \end{aligned} \tag{5}$$

where L denotes the pixel size. In the last expression, we change coordinates such that X_n becomes zero.

Figures 2, 3, 4 show the relation of X-ray events with various energies between X_{in} and $CG(X_{in})$ where we assume that the center of the nearest mesh hole is the X-ray interaction position, X_{in}. In the figures, Y axis is parallel to the charge transfer direction, which we call *vertical direction.* We employed the copper foil of $10\mu m$ thickness which blocked X-ray photons of Y-L and Ag-L from penetrating the foil. X-rays at these energies could enter only through the mesh hole, these X-rays form steep parallelogrammatic regions in the figures. The width of the region is determined by the mesh hole size while the height is determined by the split threshold level. However, the copper foil is partly transparent against the X-rays of Ti-K. Those passing through the mesh hole form a rectangular region while those penetrating the foil uniformly scatter and become background. The distribution of X-ray events shown in Figures 2, 3, 4 is not uniform along vertical direction. The top and bottom regions are dense, which shows that the charge distribution inside the cloud is concentrated in its center.

C. Charge cloud shape

We found that there was a good correlation between X_{in} and $CG(X_{in})$ both for X and Y coordinates. We fitted the data using two models for $S(\sigma, X)$ as below: eq(6) is for the Rectangular model and eq(7) is for the Gaussian model.

Rectangular model

$$S(\sigma, X) = \begin{cases} \frac{1}{2\sqrt{3}\sigma} & (\ |X| < \sqrt{3}\sigma) \\ 0 & (\ |X| > \sqrt{3}\sigma) \end{cases} \tag{6}$$

Gaussian model

$$S(\sigma, X) = \frac{1}{\sqrt{2\pi}\sigma} exp(-\frac{X^2}{2\sigma^2}) \tag{7}$$

Table II shows the results we obtained. In Table II, we also list the mean absorption length in Si, λ. The curves for the best fit models are superposed on Figures 2, 3, 4 by the solid lines for the Gaussian model

TABLE II

MODEL FIT FOR THE SPLIT EVENTS

	Y-L		Ag-L		Ti-K	
Energy (keV)	1.9		3.0		4.5	
λ (μm)	1.3		4.2		13.4	
Direction	X	Y	X	Y	X	Y
	Rectangular model					
σ (μm)	0.8±0.2	1.6±0.2	0.9±0.3	1.5±0.2	1.5±0.3	1.8±0.2
σ_{res}(μm)	2.0	1.9	2.2	2.1	3.0	2.6
elongation (σ_Y/σ_X)	2.0±0.5		1.6±0.5		1.2±0.3	
	Gaussian model					
σ (μm)	0.9±0.3	1.8±0.2	1.0±0.2	1.6±0.2	1.6±0.3	1.9±0.2
σ_{res}(μm)	2.0	1.9	2.2	2.1	3.0	2.5
elongation (σ_Y/σ_X)	2.0±0.6		1.6±0.4		1.2±0.2	

and by the dotted line for the Rectangular model. We calculated the standard deviation of the residuals, σ_{res}, between the data and the best fit model. Judging from σ_{res}, we found that there was no preference for either model. We should note that σ_{res} becomes large for Ti-K X-rays in both models. It may be due to the fact that Ti-K X-rays partly penetrate the copper foil resulting in the increase of the background while Y-L and Ag-L do not.

σ_{res} consists both of the random error and of the finite size of the mesh hole. Since the mesh hole size is about 5.6μm in diameter, we can calculate the random error which will eventually determine the accuracy of the interaction location. The effective diameter of the mesh hole is about 6μm due to the diffraction of X-rays. The expected standard deviation due to the finite size of the mesh hole will be 1.5μm. Therefore, we obtain the random error of 1.5 $\sim$ 2.2μm which represents the position accuracy of the X-ray interaction location by using our method.

IV. DISCUSSION

Our results may depend on T_{split}. Therefore, we measured the distribution for various T_{split} as shown in Figure 5. The result is summarized in Table III. We confirmed that the charge cloud size we measured is independent of T_{split} and that there is almost no difference between the Rectangular model and the Gaussian model.

Figure 6 shows the relation between the charge cloud size, σ, and the mean absorption length, λ, of X-rays in Si. There is a good positional correlation along the horizontal direction: the longer is λ, the bigger is σ. However, there is no strong correlation along the vertical direction. Charge splitting occurs due to the electric potential created below the gates. The channel stop separates the charge in the horizontal direction while the charge transfer gates separate it in the vertical direction.

We should note that the charge cloud size of the two lowest energies seems to be bigger in the vertical direction than that in the horizontal direction. This indicates that the charge isolation is worse for interphase isolation than doping-induced isolation. The elongation ratio between σ_Y/σ_X is listed in Table II. These values suggest that the charge cloud shape is elongated along the vertical direction, particularly for the X-rays with short λ. Due to the relatively large hole size in this experiment, we do not obtain clear evidence of the elongation. It should be noted that the smaller mesh hole is needed in near future experiment which will reveal the shapes in detail. The charge cloud shape measured in the multi-pitch mesh experiment shows the elongation [16], but in that case it is elongated along the horizontal direction. Our results are statistically different from theirs. This difference is probably due to the difference in the chip characteristics we used. The charge cloud shape for Ti-K is almost circular. Since the elongation of the charge cloud shape is bigger for X-rays with shorter λ, the elongation is very likely due to the complex, non-uniform field near the charge collection gates and around the channel stops. The result indicates that for Ti-K the majority of the charge diffusion occurs before confinement to the pixel level, as would be expected.

Let's consider the diffusion in a very simple model.

TABLE III

DEPENDENCE ON T_{split} FOR Y-L Y-DIRECTION

T_{split} (eV)	120	90	60
	Rectangular model		
σ (μm)	1.6±0.2	1.7±0.2	1.7±0.2
σ_{res}(μm)	1.9	1.9	1.9
	Gaussian model		
σ (μm)	1.8±0.2	1.9±0.2	1.8±0.2
σ_{res}(μm)	1.8	1.9	1.8

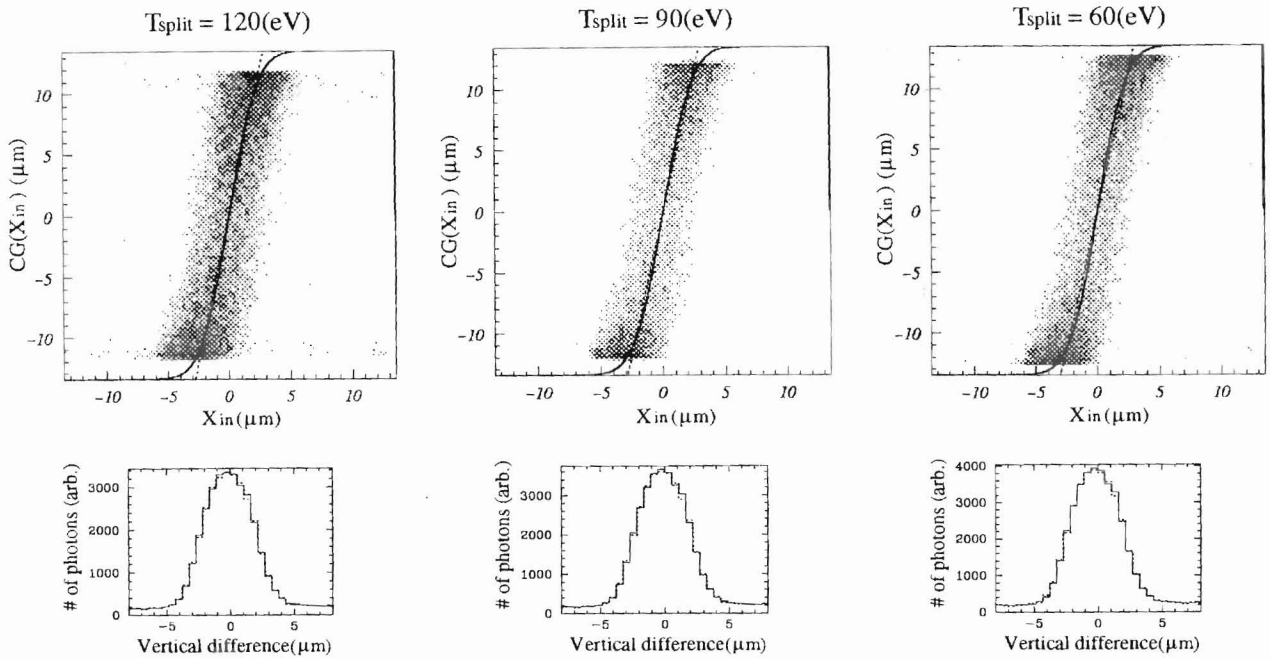

Fig. 5. The relation of Y-L X-ray events with various split threshold level between X_{in} and $CG(X_{in})$.

The characteristic diffusion size of the charge cloud, L_D, is proportional to $\sqrt{t} \sim \sqrt{\frac{\lambda}{\mu E}}$, where t is the travel time, μ is the electron mobility in Si and E is the mean electric field strength inside the depletion region. Therefore, L_D is roughly proportional to $\sqrt{\lambda}$. At the energies used in our experiments, the diffusion is the dominant factor determining the charge cloud size and we can consider L_D as σ. Based on our result, we can expect that σ will be 2.4μm for 5.9 keV and 3μm for 8.04 keV, respectively. When the charge cloud size becomes large, the fraction of the split events increases meaning that the region generating the split events expands. Since we show that we can improve the X-ray interaction position for split events, we can obtain much finer position for relatively high energy X-rays if they are photoabsorbed in the depletion region. Those photoabsorbed in the field free region will form wide spread events can be excluded from the event pattern recognition.

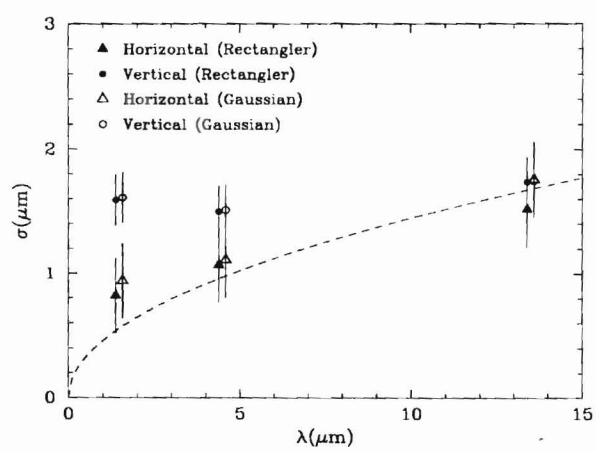

Fig. 6. The relation of the charge cloud size (σ) is plotted against λ in Si. Dashed line shows the relation of $\sigma \sim \sqrt{\lambda}$.

The various X-ray events are produced in specific areas inside the pixel [11], [14], [15]. Single events are confined in a central region of the pixel while split events occur in a boundary region of the pixel. Figure 7 shows the mini-pixel regions [15] in which the X-rays become single and split events. The width of the split region will increase as the X-ray energy increases. As given in eq.(6), the width of the split region is about $2\sqrt{3}\sigma$. There are four types of mini-pixels in the CCD pixel which corresponds to event types shown in Figure 1. The mini-pixel corresponding to the single events is the region in which we can not determine the interaction position better than the mini-pixel size. The mini-pixel corresponding to the horizontal (vertical) split events is the region in which we can determine the interaction position along the horizontal (vertical) direction better than the mini-pixel size. The region corresponding to the 3–4 pixel events is the region in which we can specify the interaction position both along the horizontal and the vertical directions better than the mini-pixel size. The actual charge cloud size will depend on the CCD chip and its operating conditions. However, our result is

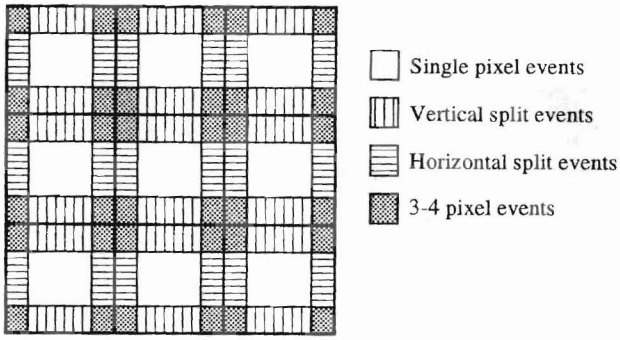

Fig. 7. A schematic view of 3×3 pixels is shown with mini-pixel boundaries. The mini-pixel in the pixel center generates the single event while surrounding mini-pixels generate the split events. Pixel boundary is drawn with thick lines.

applicable to different types of CCD as a first approximation.

Based on the calibration of AXAF CCD whose pixel size is 24μm, the fraction of single events is about 25% at 7.5 keV [17] and decreases at higher X-ray energy. The split event width is about 12μm at 7.5 keV. In this case, we will obtain the position accuracy of $\pm 6\mu$m for single events and a few μm accuracy for split events. In the photon counting CCD, pileup can be serious problem which prevents us to improve the determination of the X-ray interaction position. Therefore, our method is valid only when the X-ray intensity is weak enough that the pileup does not become serious.

V. Conclusion

We performed a single-pitch mesh experiment using the CCD with a pixel size of 27μm square. There are two types of X-ray events: single events and split events. We performed the mesh experiment and determined the interaction location for each X-ray photon. We found that the center of gravity of the split event was well correlated with the interaction location with subpixel resolution. Accurate X-ray interaction position can be obtained by calculating the center of gravity of the event weighted by the charge. The charge cloud shape determines the conversion formula from the center of gravity to the actual interaction position. We can not distinguish between Gaussian models and Rectangular models of the charge cloud shape. We analyzed the data using the both models and found that the charge cloud size is $1 \sim 2\mu$m for the X-rays we used.

The accuracy of the X-ray interaction location that can be achieved is about $1.5 \sim 2.2\mu$m for split events. The corresponding accuracy for single events is the size of the mini-pixel region showed in Figure 1. It is also less than the pixel size. Therefore, we can achieve the subpixel spatial resolution for any X-ray events.

Acknowledgments

We want to express our thanks to Dr. P. Serlemitsos who arranged for us to use the X-ray beam line and the CCD. HT and KY are partly supported by the HEASARC.

References

[1] G. W. Frazer, *X-ray Detectors in Astronomy*, Cambridge, Cambridge University press, 1989, p. 208.

[2] Y. Tanaka, H. Inoue and S. S. Holt, "The X-ray astronomy Satellite ASCA", *Publ. Astron. Soc. Jpn.*, vol. 46, pp. L37-L41, 1994.

[3] M. C. Weisskopf, S. L. O'Dell, R. F. Elsner and L. P. Van Speybroeck, "Advanced X-ray Astrophysics Facility (AXAF): an overview", *Proc. SPIE*, vol. 2515, pp. 312-329, 1995.

[4] M. C. Weisskopf and S. L. O'Dell, "Calibration of the AXAF observatory: overview", *Proc. SPIE*, vol. 3113, pp. 2-17, 1997.

[5] P. Barr et al., ESA SP-1097, Mar. 1988.

[6] O. Citterio, P. Conconi, M. Ghigo, F. Mazzoleni, R. Buzzi and G. Parodi, "Use of ceramic materials for lightweight x-ray optics", *Proc. SPIE*, vol. 3113, pp. 334-341, 1997.

[7] H. Inoue, "The Next generation of X-ray observatories", *Proc. Leicester X-ray Astronomy Group Special Report XRA97/02*, p. 161, 1997.

[8] A. A. Wells et al., "X-ray imaging performance of the flight model JET-X telescope", *Proc. SPIE*, vol. 3113, pp. 392-403, 1997.

[9] G. Richter et al., L. Bassani, G. di Cocco (eds.), *Imaging in High Energy Astronomy. Experim. Astron.*, p. 159, 1996.

[10] P. Friedrich, G. Hasinger, G. Richter, K. Fritze, J. Trümper, H. Bräuninger, P. Predehl, R. Staubert and E. Kendziorra, MPE Report, vol. 263, p. 681, 1996.

[11] H. Tsunemi, K. Yoshita, and S. Kitamoto, "New Technique of the X-ray Efficiency Measurement of a Charge-Coupled Device with a Subpixel Resolution", *Japan J. Appl. Physic*, vol. 36, p. 2906 ,1997.

[12] H. Tsunemi, J. Hiraga, K. Yoshita and S. Kitamoto, "Where Are the X-ray Event Grades Formed Inside the Pixel of the Charge-Coupled Device? The Behavior of the Primary Charge Cloud Inside the Charge-Coupled Device", *Japan J. Appl. Physic*, vol. 37, pp. 2734-2739, 1998.

[13] B. E. Burke, R. W. Mountain, P. J. Daniels, M. J. Cooper and V. S. Dolat, "CCD Soft X-ray Imaging Spectrometer for the ASCA Satellite", *IEEE Trans. Nucl. Sci.*, vol. 41, pp. 375-385, 1994.

[14] K. Yoshita, H. Tsunemi, K. C. Gendreau, G. Pennington and M. W. Bautz, "Direct Measurements at the Sub-pixel Level of the X-ray Detection Efficiency of the CCD on board the ASCA satellite", *IEEE Trans. Nucl. Sci.*, vol. 45, pp. 915-920, 1998.

[15] M. J. Pivovaroff, S. Jones, M. Bautz, S. Kissel, G. Prigozhin, G. Ricker, H. Tsunemi and E. Miyata, "Measurements of the Subpixel Structure of AXAF CCD's", *IEEE Trans. Nucl. Sci.*, vol. 45, pp. 164-175, 1998.

[16] H. Tsunemi, J. Hiraga, K. Yoshita and K. Hayashida, *Nucl. Instr. and Meth*, (1998) submitted.

[17] M. Nishiuchi, K. Koyama, T. G. Tsuru, H. Awaki, H. Tomida, K. Hamaguchi and H. Tsunemi, "The response function of an X-ray CCD camera onboard the Astro-E satellite", *Proc. SPIE*, vol. 3445, pp. 268-277, 1998.

[18] K. C. Gendreau, Ph. D thesis, MIT, 1995. Available from http://lheawww.gsfc.nasa.gov/~kcg/thesis/thesis.html.

4075544